VERSITA

Biologia **64**/1: 27—42, 2009
Section Cellular and Molecular Biology
DOI: 10.2478/s11756-009-0013-y

Quantitative analysis of time-series fluorescence microscopy using a spot tracking method: application to Min protein dynamics

Somrit Unai[1]*, Paisan Kanthang[1]*, Udorn Junthon[1], Waipot Ngamsaad[1], Wannapong Triampo[1,2,3]**, Charin Modchang[1] & Chartchai Krittanai[4]

[1] *R&D Group of Biological and Environmental Physics, Department of Physics, Faculty of Science, Mahidol University, Rama 6 Rd., Ratchatewee, Bangkok 10400, Thailand; e-mails: scwtr@mahidol.ac.th or wtriampo@gmail.com*
[2] *Center of Excellence for Vector and Vector-Borne Diseases, Faculty of Science, Mahidol University, Nakhonpathom, Thailand*
[3] *Institute for Innovation and Development of Learning Process, Mahidol University, Bangkok, Thailand*
[4] *Institute of Molecular Biology. and Genetics, Mahidol University, Nakhonpathom, Thailand*

Abstract: The dynamics of MinD protein has been recognized as playing an important role in the accurate positioning of the septum during cell division. In this work, spot tracking technique (STT) was applied to track the motion and quantitatively characterize the dynamic behavior of green fluorescent protein-labeled MinD (GFP-MinD) in an *Escherichia coli* system. We investigated MinD dynamics on the level of particle ensemble or cluster focusing on the position and motion of the maximum in the spatial distribution of MinD proteins. The main results are twofold: (i) a demonstration of how STT could be an acceptable tool for MinD dynamics studies; and (ii) quantitative findings with parametric and non-parametric analyses. Specifically, experimental data monitored from the dividing *E. coli* cells (typically 4.98 ± 0.75 μm in length) has demonstrated a fast oscillation of the MinD protein between the two poles, with an average period of 54.6 ± 8.6 s. Observations of the oscillating trajectory and velocity show a trapping or localized behavior of MinD around the polar zone, with average localization velocity of 0.29 ± 0.06 μm/s; and flight switching was observed at the pole-to-pole leading edge, with an average switching velocity of 2.95 ± 0.31 μm/s. Subdiffusive motion of MinD proteins at the polar zone was found and investigated with the dynamic exponent, α of 0.34 ± 0.16. To compare with the Gaussian-based analysis, non-parametric statistical analysis and noise consideration were also performed.

Key words: spot tracking; *E. coli*; cell division; Min proteins; MinD; protein oscillation.

Abbreviations: GFP-MinD, green fluorescent protein-labeled MinD protein; MTS, membrane-targeting sequence; MSD, mean squared displacement; PSD, power spectrum density; ROI, region of interest; SPT, single particle tracking; STT, spot tracking technique; Z-ring, equatorial ring.

Introduction

In *Escherichia coli* and other rod-shaped bacteria, cell division depends on the precise placement of a division septum in the middle of the cell, a process initiated by the assembly of an equatorial ring (Z-ring) of the tubulin-like FtsZ GTPase on the cytoplasmic membrane (Lutkenhaus & Addinall 1997; Rothfield et al. 1999). The Z-ring assembly is spatially restricted to midcell by nucleoid occlusion (Woldringh et al. 1991; Yu & Margolin 1999) and by the dynamics of the Min system (de Boer et al. 1989; Rothfield et al. 2001). Nucleoid-free zones provide for the possible placement of the Z-ring within three regions – two polar zones and a midcell zone – while the Min system prevents Z-ring assembly at the polar zone. The Min system consists of the MinC, MinD, and MinE expressed from the *minB* operon (de Boer et al. 1989) which restricts separation to the desired potential division site at the midcell through the oscillatory cycle from pole to pole (reviewed in Rothfield et al. 2005). *In vivo*, MinC co-localizes and co-oscillates with MinD (Hu & Lutkenhaus 1999; Raskin & de Boer 1999a) which acts together as a negative regulator of Z-ring assembly, and oscillatory dynamics depends on MinE (Hu & Lutkenhaus 1999; Raskin & de Boer 1999a,b). MinCD complex prevents the correct interaction of FtsA with the FtsZ ring *in vivo* (Justice et al. 2000), and MinC has been shown to inhibit FtsZ polymerization *in vitro* (Hu & Lutkenhaus 1999).

With regards to Min protein dynamics both *in vitro* and *in silico*, a considerable number of experiments have been done. Computationally, several studies have been carried out with different reaction-diffusion

* Co-first authors
** Corresponding author

Springer

models to explain these oscillations (Howard et al. 2001; Meinhardt & de Boer 2001; Kruse 2002; Howard & Rutenberg 2003; Huang et al. 2003; Modchang et al. 2005). It has also recently emerged that MinD forms helical filaments in living cells (Shih et al. 2003) and recent mathematical models (Drew et al. 2005, Pavin et al. 2006) have attempted to include this feature. The model by Drew et al. (2005) includes polymer growth from nucleation sites at the ends of the cell. Both of these models use continuous partial differential equations. The model by Pavin et al. (2006) differs in that it is a three-dimensional stochastic model, but it does not yield the observed large scale helical filaments. Incorporating stochastic feature introduced into Min modeling is nevertheless likely to be important for systems of this type (Howard & Rutenberg 2003; Fange & Elf 2006; Pavin et al. 2006; Tostevin & Howard 2006). Although almost all previous findings were able to provide both qualitative and quantitative predictions, only qualitative ones were verified, mainly due to the lack of quantitative experimental data. Therefore, a more quantitative approach is urgently required.

Most experiments have focused on assembly and dynamics especially the spatial-temporal pattern formation and periods of the MinCDE system. An excellent overview has been given by Lutkenhaus (2007). In terms of technique-based approaches, most work has used fluorescent proteins: selectively labeled single proteins together with high-resolution fluorescence imaging which is made possible by a new generation of bright-field and confocal microscopes (Hu & Lutkenhaus 1999; Raskin & de Boer 1999b; Rowland et al. 2000; Hale et al. 2001; Rothfield et al. 2001; Szeto et al. 2002; Shih et al. 2003). Of particular interest is the work by de Boer et al. (1991) who studied the localization of MinD by monitoring membrane-associated protein of MinD in fixed *E. coli* cells. In conjunction with immunoelectron microscopy, anti-MinD antiserum and colloidal gold-labeled second antibodies were used to reveal MinD associated with the cytoplasmic membrane. However, most results are mainly qualitative. The precision of the green fluorescent protein GFP-MinD or GFP-MinE data – in terms of positions, velocity, trajectory, and so on – could be improved upon.

To precisely track the positions in time-series of the region of interest (ROI) of Min proteins (provided by GFP-Min protein signals), the following conditions must be met: (1) the image-capturing equipment must be fast enough; (2) the stages or samples must be stable enough to prevent frame-shift at small scales; (3) the noise or thermal fluctuation must not be very large; and (4) the fluorescent signal must last long enough to provide reliable and intelligible data. Indeed, based on the four above-mentioned conditions, most experimental works published so far on the Min system seem to satisfy these criteria. Here, applying the spot tracking technique (STT) to particle ensemble of MinD proteins, referred to as STT, for quantitative study of the spatial-temporal pattern and the dynamics of MinD is one of our main focuses, in addition to the MinD dynamics itself.

STT that occurs in this report has the same feature with the single particle tracking (SPT). That technique is a computer-enhanced video microscopy that has been developed to measure not only the movement of single small molecules or particles, but also the trajectories of the molecule ensembles (Qain et al. 1991; Saxton & Jacobson 1997). Mostly it is used to track the motion of proteins or lipids on the cell surface – individual molecules or small clusters with a typical spatial resolution of tens of nanometers and a typical time resolution of tens of milliseconds. SPT has been used mostly in data analysis in order to classify the modes of motion (e.g., normal diffusion, anomalous diffusion, confined motion, etc.) and to find the distribution of quantities characterizing the motion. As mentioned earlier, the data from SPT measurements generally constitute an important key for characterization of the cell membrane. Hence, it is not only a probe of the membrane microstructure, but it can also contribute significantly to the study of reaction kinetics within the cell membrane. The SPT technique has been used in a large field of biophysical research, such as in plasma and nuclear membrane studies (Saxton & Jacobson 1997), nuclear trafficking of viral genes (Babcock et al. 2004), chromosome dynamics (Sage et al. 2005) and bacterial actins motion (Kim et al. 2006).

Motivated by the above mentioned considerations, this work has been devoted to the adaptation of the STT for the quantitative study of Min protein dynamics. To the best of our knowledge, this is the first time ever that the STT has been applied to this particular MinD dynamics problem: the focus being on the dynamics and localization of MinD protein pole-to-pole oscillations. As shall be seen later, our results not only will demonstrate how to apply STT to the MinD system, but also will confirm all previous qualitative results. This could be used to provide, for example, characteristic time-scale, reaction rate, diffusion coefficient, and so on. Hence, with regards to Min protein dynamics, not only can qualitative information be obtained with this STT, but much more direct quantitative information may be obtained as well. This will allow us to answer more precisely and specifically the crucial questions associated with these phenomena; for example: how do particle ensembles move on the cell surface, and how are the proteins assembled? Our results can potentially bridge the gap between the *in silico* and *in vitro* or *in vivo* experiments.

Material and methods

Bacterial strain and growth conditions

E. coli RC1/pFX9 [$\Delta min/P_{lac}$-*gfp*::Δ*minD* Δ*minE*] was kindly provided by Yu-Ling Shih of the Department of Microbiology, University of Connecticut Health Center (Shih et al. 2003). For examination of MinD labeled with GFP, a starter of RC1/pFx9 cells was grown in LB medium containing 50 μg/mL ampicillin, 25% glucose, at 37°C and shaken at 250 rpm overnight. Then 1% of the overnight

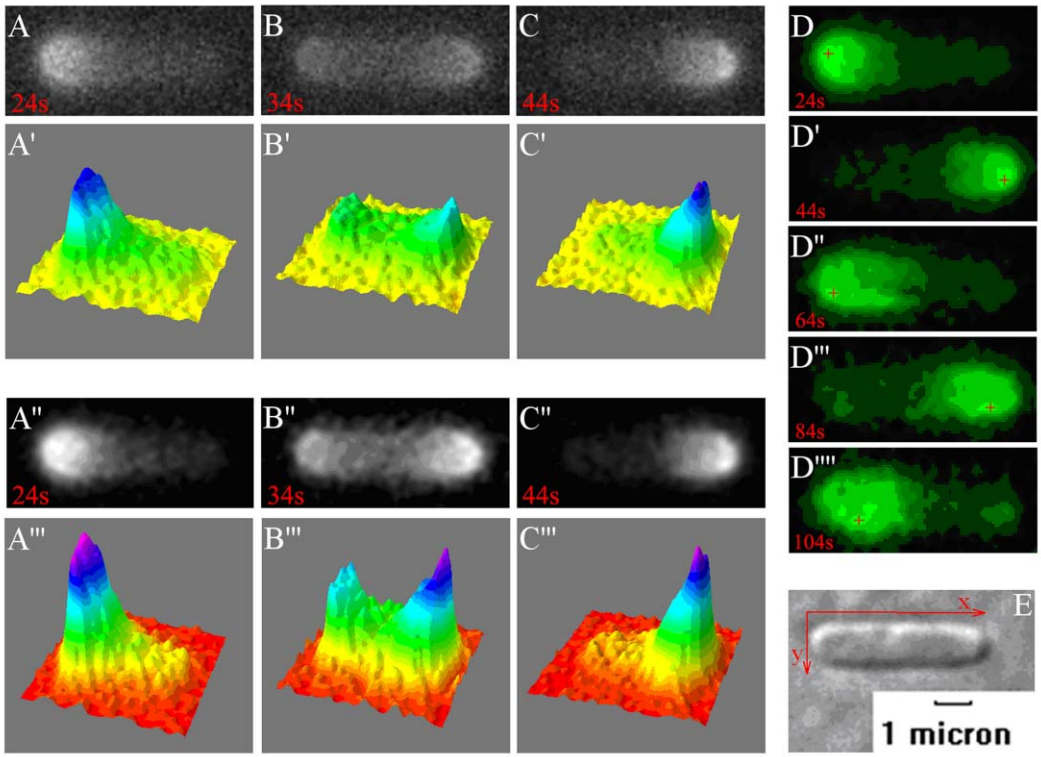

Fig. 1. Image processing and SpotTracking results for RC1 *E. coli* cell [*min*/P_{lac}-*gfp::minD minE*]. (**A**), (**B**) and (**C**) shows raw fluorescent images at times 24 s, 34 s, and 44 s. (**A**′), (**B**′) and (**C**′) shows intensity plot of fluorescent images corresponding to (**A**), (**B**) and (**C**). (**A**″, (**B**″) and (**C**″) shows fluorescent images of (**A**), (**B**) and (**C**) after filtering with Gaussian blur and rescaling. (**A**‴), (**B**‴) and (**C**‴) shows intensity plot of images (**A**″), (**B**″) and (**C**″). (**D**), (**D**′), (**D**″), (**D**‴) and (**D**⁗) shows fluorescent images after tracking with SpotTracker at time 24 s, 44 s, 64 s, 84 s, and 104 s. The positions of ROI are indicated by red cross sign. (**E**) shows a DIC image (gray), cell length ∼5 μm.

culture was taken to grow in the new medium until the OD_{600nm} was approximately 0.4. Centrifugation was performed at 3,000 rpm for 15 min to collect the cells. Cells were then re-suspended in the same medium containing 0.1 mM isopropyl-β-D-thiogalactopyranoside (IPTG) for protein induction. The cell culture was diluted with media before use.

Image acquisition

For fluorescence image sequences, a Zeiss Axioskop2 microscope and A-plan 100x/1.25 oil lenses were used with InVivo software support with exposure times of 900 ms. A charge-coupled device (CCD) camera (Evolution QEi monochrome) was attached to the video port of the microscope to acquire images and movies at 1 frame/s. In our experimental preparation, 5–7 μL of sample was dropped onto a glass slide coated with 5 μL poly-L-lysine (0.1%), and then covered by a cover slip at room temperature (25 ℃) before examination.

Image processing and STT

STT was used to follow the ROI which gives off the highest GFP-MinD concentration signal. This highest intensity is the representation of MinD ensemble in the cell. The data obtained from measurements are supported by the SpotTracker Java plug-in for the public domain ImageJ software (http://rsb.info.nih.gov/ij/). SpotTracker (http://bigwww.epfl.ch/sage/soft/spottracker/) is a robust and fast computational procedure to track fluorescent particles attached to the molecule of interest in time-lapse microscopy.

The tracking process was performed in three steps, as follows. Firstly, the *E. coli* cell in the raw fluorescence image sequence was rotated lengthwise along the major axis (x-axis), as shown in Figure 1A–C. The goal of rotating the cell is to properly align it for image analysis, since the protein behavior is due to MinD oscillations from pole to pole along the cell length. However, at this stage the acquired image sequences (as shown in Figure 1A–C) are full of noise resulting from thermal fluctuation and the fading of fluorescence signals (typically after about 4–5 min). Realizing that this effect could reduce the accuracy of GFP-MinD ensemble positions collected from SpotTracker, or lead to misinterpretation of the GFP-MinD phenomenon, the images obtained must be further processed using a Gaussian filter with 2-pixel radius in order to reduce the effect of noises. It should be noted that if the pixel radius is too large, the positions of ROI are not accurate. The corresponding intensity plot after reducing the noise is shown in Figure 1A′–C′. Next, the low noise and signals were enhanced by using the SpotTracker rescaling option. One possible area of concern regards the filters used. We feel that this would be a promising area of research which could ultimately improve the quality of the filtering procedure. As a consequence of the image enhancement process, the enhanced image, seen in Figure 1A″–C″, shows a better GFP signal than the raw fluorescence images in Figure 1A–C. The associated intensity signal is also shown in Figure 1A‴–C‴. As can clearly be seen, a consequence of the noise reduction is to make the region of high intensity more apparent. Next, the tracking procedure of ROI was performed, again using the SpotTracker plug-in. This tracking provides the time series data for the position

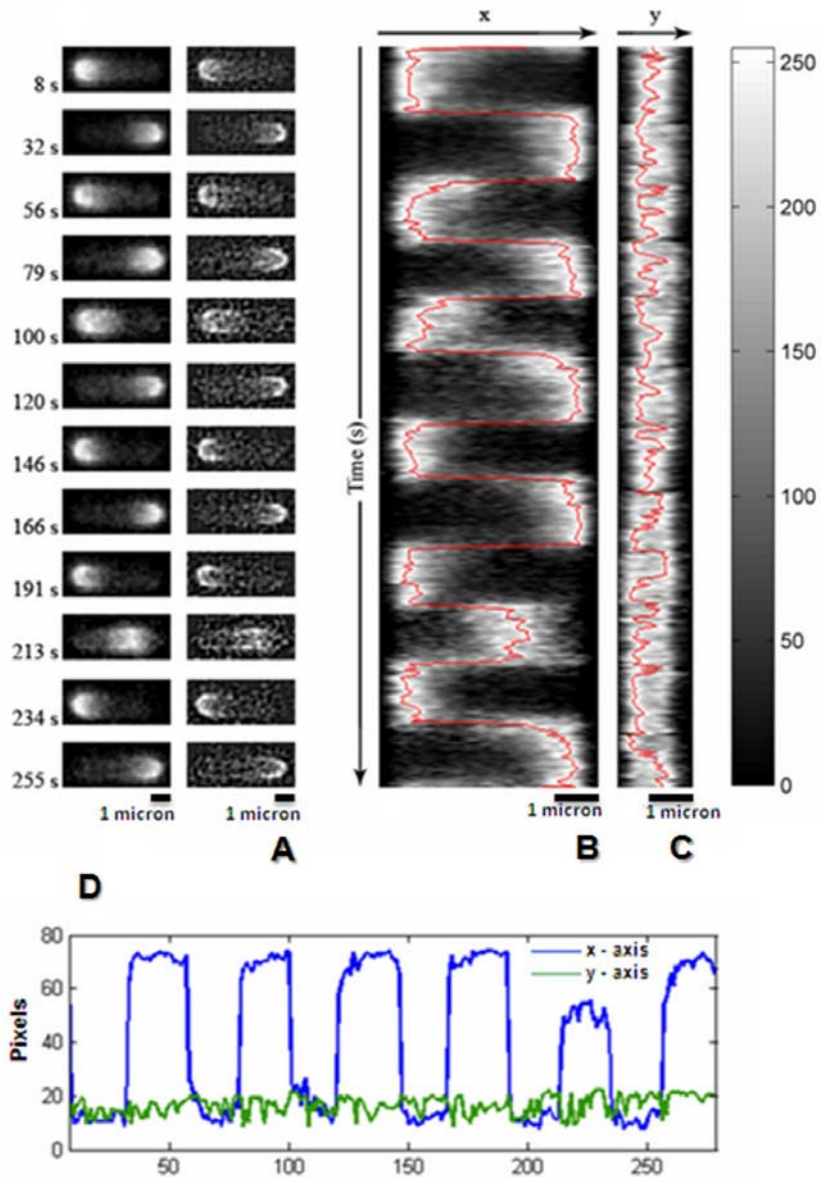

Fig. 2. The ensemble GFP:MinD oscillations from pole to pole between 8 s to 279 s with period of approximately 45 seconds. (**A**) The 2D image sequence of pole-to-pole MinD oscillations at each successive time for the rescaled and enhanced signal are shown on the left and the right columns, respectively. Each fluorescent image represents the ensemble of GFP:MinD signal locating at polar zones. The labeled time on the left side of column is the first time of GFP:MinD assembles after switching to new pole. (**B**) The results of SPT show the GFP signal time evolution trajectory of MinD oscillations on $x(t)$. The red line represents the ensemble of GFP:MinD trajectory. **(C)** Spot projection on $y(t)$ of GFP signal time evolution trajectory of MinD oscillations. **(D)** Time evolution plot of the position on x axis (blue line) and y axis (green line).

of ROI of the GFP-MinD system as a text file (x, y coordinates), as shown in Figure 1D–D′′′′. In this figure, red crosses indicate the ensemble positions at the highest intensity signal. Finally, the ensemble positions were analyzed by MATLAB software to calculate physical quantities including velocity, period, and probability distribution. In fact, other dynamic quantities could also be calculated via this method. More details of this tracking as a time algorithm can be found in Sage et al. (2005).

Results and discussion

Here we have applied the STT to experimentally and quantitatively investigate the dynamics in the assembly of MinD proteins. By using a combination of the STT and image processing, we were able to demonstrate the redistribution pattern of GFP-MinD (as a mirror reflection of MinD proteins). Having focused on the dynamic behavior of MinD protein molecules, their moving positions were then traced by high-intensity region, as shown in Figs 1A′′–C′′ and 1A′′′–C′′′. The STT measurements provided the x and y coordinates for the center of ROI (visualization of ROI centers is shown in Figure 1D–D′′′′). The sequence of positions (x, y) at successive times can be used to determine the trajectory of GFP-MinD in x and y components, as shown in Figure 2B and 2C, respectively.

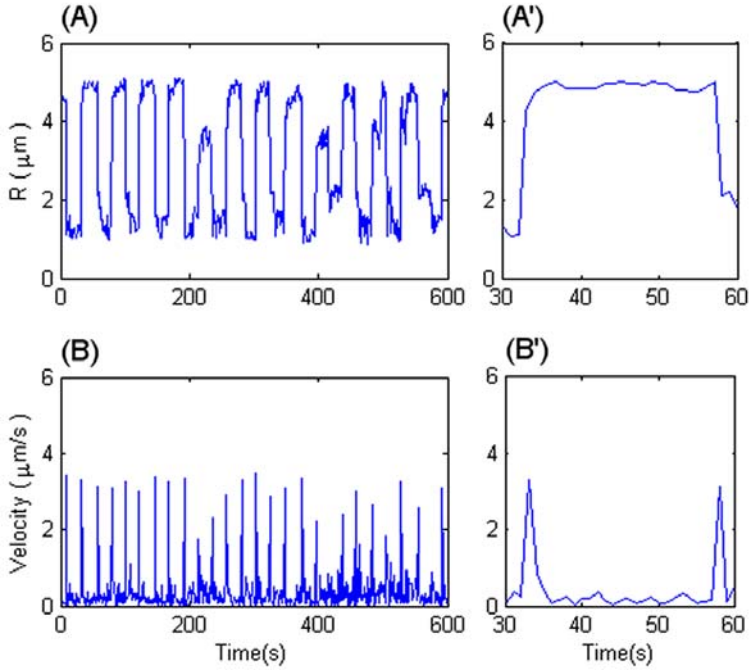

Fig. 3. The comparison of the time evolution dynamics between distance and velocity of *E. coli* cell for 600 seconds. (**A**) shows time evolution of $R = \sqrt{(\Delta x)^2 + (\Delta y)^2}$ and **(A')** shows subplot of R for the time interval 30–60 seconds. The distance as a function of time shows the oscillatory dynamics from pole to pole. (**B**) and (**B'**) show the velocity-time evolution throughout the time interval, and during a subinterval in time, respectively. The velocity as a function of time shows the switching velocity for each peak in (**B**) and localization velocity between peak to peak.

Pole-to-pole oscillatory dynamics of GFP-MinD

Analysis of the high-intensity regions in each frame of the image sequences using an enhanced filter (right column of Figure 2A) reveals the pole-to-pole oscillatory dynamics pattern between the polar zones. So far, this is qualitatively consistent with previous findings, which have used both experimental (de Boer et al. 1991; Hu & Lutkenhaus 1999; Raskin & de Boer 1999b; Rowland et al. 2000; Hale et al. 2001; Szeto et al. 2002, 2005; Shih et al. 2003) and theoretical methods (Howard et al. 2001; Meinhardt & de Boer 2001; Kruse 2002; Howard & Rutenberg 2003; Huang et al. 2003). More importantly, using the extracted (x, y) allows us to precisely locate the positions of the MinD at a given time (Fig. 2D), portraying its trajectory.

The results from the STT provide us with information on position alterations and time sequences that can be used to analyze the GFP-MinD motion in two ways: (i) how the trajectory reflects the positional behavior of cluster proteins as depicted in Figs 3A and 3A′; and (ii) how the velocity time evolution features movement behavior of cluster proteins as in Fig. 3B and 3B′. Both results can indeed bring about the same information regarding the phenomenological characteristics of cluster protein motion. Typically, the characteristics of GFP-MinD protein dynamics can be classified, according to the space and time scale of dynamic events, into two types: trapping events and flight events. Trapping events mostly occur at the polar zones, while flight events take place in between the trapping events in the space between the polar zones.

For trapping events, it is evident from the data that the ensemble GFP-MinD trajectory positions change very little (≤10%) during this state, as shown in Figs 3A and 3A′. Likewise, the velocities during those time intervals change very little from peak to peak, as shown in Figs 3B and 3B′. This dynamic information implies that MinD positions typically take a relatively long time at the polar zones (∼ 27 s) while flight events take considerably lesser time (∼2–4 s). Therefore, high concentrations of GFP-MinD are mostly found in the polar regions (Fig. 2B). We have learned from previous studies that the dynamics of trapping events at polar zones are believed to correspond to polar zone growth by the formation of MinD polymerization at the cytoplasmic membrane (Hu et al. 2001; Suefuji et al. 2002). It is also possible that MinD may interact with itself or with other Min proteins or cytoplasmic components in a complicated manner not yet well understood. One reaction diffusion model by Huang et al. (2003) has proposed that this behavior is due to "cycling" of MinD in the polar zone, whereby molecules repeatedly unbind and then quickly rebind. For flight event dynamics, as previously mentioned, typical characteristics are that the positions of the proteins quickly change from pole to opposite pole during a specific time interval. This dynamic behavior is clearly evidenced by the switching velocity, which corresponds to the peaks of each time interval mentioned earlier, as shown in Figs 3B and 3B′. Comparatively, the velocities associated with flight events are much higher than the velocities at the polar zone (∼ tenfold). During this state, as briefly mentioned in the Introduction, when MinE in the E-ring activates the ATPase activity of MinD:ATP molecules to undergo

hydrolysis, it results in the release of MinD:ADP, MinC and MinE products from the membrane into the cytoplasm (Hu & Lutkenhaus 2001; Hu et al. 2002; Suefuji et al. 2002; Rothfield et al. 2005). The MinE thus immediately sweeps MinD out of the midcell, allowing the Z-ring to form. The Z-ring assembly is spatially restricted to the midcell by nucleoid occlusion (Woldringh et al. 1991; Yu & Margolin 1999) and by the MinCDE system (de Boer et al. 1989; Rothfield et al. 2001). The first mechanism ensures that Z-rings form only in cellular space devoid of nucleoid mass, while the Min system prevents Z-ring assembly at the cell poles. This process is repeated when MinD:ADP is converted to MinD:ATP in the cytoplasm and continually diffuses to the opposite pole, thereby giving rise to the flight events and velocity switching.

Oscillatory period

From trajectory and velocity profile (Figs 2, 3), we can measure the average period of GFP:MinD ensemble that travels between the two polar zones of a cell. This oscillating period can be precisely determined either from the trajectory cycle along x-axis displacement (Figs 3A and 3A′) or the cycling peaks of velocity time evolution (Figs 3B and 3B′). Here we used the latter to find the period which corresponds to the two times of the average time interval between the two successive switching velocities. We defined the switching index to be the ordinal marker of the switching event occurring as the time progresses. The switching time interval related to the switching index in more or less linear way (as shown in Fig. 4A). The slope of a graph in Figure 4A provides the half oscillation period for each individual cell. Hence with these quantitative data via STT of GFP:MinD, it provides oscillatory periods of MinD which could be more accurate than those obtained by other direct count methods. However, the obtained periods seem fluctuating as shown in Figure 4B that represents the period vs. cell length. Generally, this phenomenon could be due to biological or methodological contribution or both. Noises are somewhat well known factors as well. Our calculations yield an average oscillating period of 54.6±8.6 seconds when averaging over 13 individual cells with an average length of 4.98 ± 0.75 μm. The actual cell length used was recorded between 4 and 6μm, and periods range from approximately 45 to 65 s. Remarkably, our oscillating period of MinD is consistent with those obtained in previous reports (Hu et al. 1999; Raskin et al. 1999a; Hale et al. 2001; Shih et al. 2003; Szeto et al. 2005) as shown in Table 1. Moreover, the oscillation period was found somehow to depend on the cell length especially for the length around 4.8–5.6 μm (Fig. 4B). A comparison of this period with other reported data once again is shown in Table 1. It is speculated that oscillation periods may be varied depending on several factors, such as protein concentrations, the strains of *E. coli* cells, attachment of fluorescent or tag proteins, and other biological factors. The biophysical relationship between protein oscillation and the affecting factors is exceptionally challenging research work.

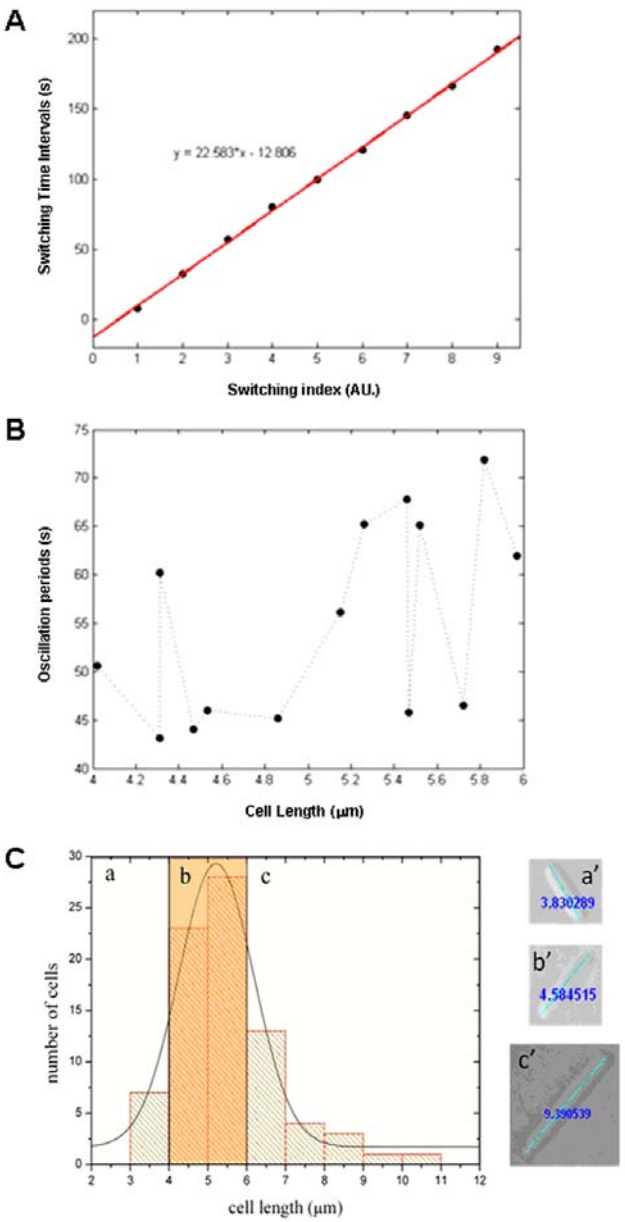

Fig. 4. Switching time intervals and oscillation periods. (**A**) The switching time intervals plot to calculate the period of pole-to-pole oscillation for an *E. coli* cell. The solid line fits to linear; period = 2*slope. (**B**) The relation between oscillation period and cell length (4–6 μm). These cell samples are not the striped oscillatory pattern appears. (**C**) The cell size distribution was performed in our experiments. The non-striped oscillation pattern indicated at the **b**-region. In addition, **a** and **c** regions indicate the short oscillation time and the striped oscillation pattern respectively. For **a'**, **b'** and **c'** represent the cell sample according to the distribution zone **a**, **b** and **c**, respectively.

It is reasonable to say that this quantitative information could contribute to an improvement of the dynamic model of the protein oscillation. Our findings reveal more understandings about protein motions which play an important part in their function. It is important to emphasize that having been able to obtain the quantitative data of protein dynamics is one of the distinct rewards owing to this applied STT. Of course precision of our results could well be affected by the sensitivity of

Table 1. Oscillation cycle period(s) corresponding to each bacterial strain.

Strain/Plasmid	Genotype	Oscillation cycle period (s)	Reference
PB103(λDR122)	*wt*(P_{lac}::*gfp-minDE*)	∼ 34	Raskin et al. (1999a)
PB103/pDR122	*wt*/P_{lac}::*gfp-minDE*	∼ 38	Raskin et al. (1999a); Hale et al. (2001)
PB114(λDR122)	Δ*minCDE*(P_{lac}::*gfp-minDE*)	∼ 40	Raskin et al. (1999a)
HL1/pDB213	Δ*minDE*/P_{lac}::*gfp-minD*, *minE-bfp*	∼ 55	Hale et al. (2001)
pWM1255	P_{trc}::*gfp–minD*$_{Ec}$, *minE*$_{Ec}$	∼ 37	Ramirez-Arcos et al. (2002)
HL1/pFX40	Δ*minDE*_P_{lac}-*yfp*::*minD*, *minE*	∼ 60	Shih et al. (2003)

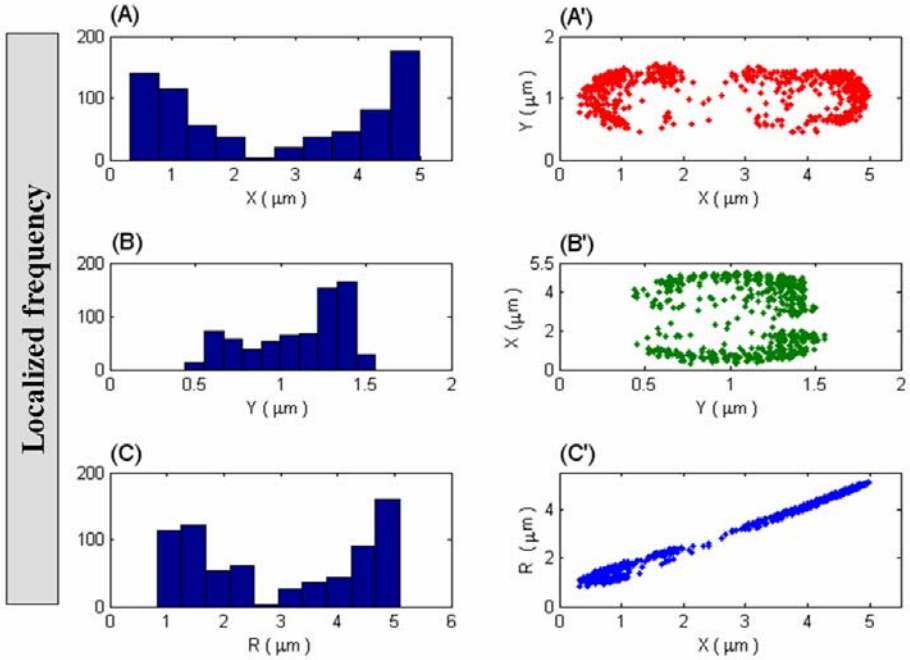

Fig. 5. The histogram and position scattering of GFP:MinD localization during 600 second time interval. (**A**), (**B**) and (**C**) are histograms that represent the localized frequency of GFP:MinD along x, y and R, respectively. (**A**′), (**B**′) and (**C**′) show the position scattering plotsof x-y, y-x and R-x, respectively.

detection or noises besides systematic errors and other stochastic effects.

GFP:MinD localization

Knowing a protein's localization helps elucidate its function. For the MinD protein this localization likely provides more understanding of how *E. coli* can archive the accurate cell division. Physically, one may understand the localization of proteins through the concepts of a dynamic instability and energy. Here we have analyzed ensemble GFP-MinD localization through the histogram plots shown in Figure 5A–C and the position-scattering plots shown in Figure 5A′–C′. The data were collected during a 600 s time interval. Along the x-axis (or along the poles), it is clearly seen that MinD proteins mostly distribute and localize in the vicinity of the poles. This is spatially depicted by a two-dimensional scattering plot. On the other hand, the region near the midcell has a lower concentration of MinD, as previously reported (Hu & Lutkenhaus 1999; Raskin & de Boer 1999a,b; Hale et al. 2001). To our knowledge, this is the first time that the time-averaged concentration of MinD (or division inhibitor) has been experimentally and quantitatively revealed to be lowest at midcell (as was qualitatively known before). Accordingly, through the STT technique, we are provided with quantitative data of how local densities of MinD are distributed. This information could be of great value in predicting the specific sites of localization and the reactions of MinD. Concerning the observed spatial inhomogeneity of MinD from previous findings (Howard & Rutenberg 2003; Fange & Elf 2006; Kerr et al. 2006; Pavin et al. 2006; Tostevin et al. 2006), it was theorized that this is due to the helical movement during the Min protein polymerization. Therefore, when a vertical section of *E. coli* is performed, many tracked spots would be seen mostly on the top and at the bottom, at somewhat constant intervals (data not shown). This phenomenon is expected to be clearly seen when using real-time three-dimensional image-capturing and reconstruction techniques such as confocal microscopy. Once again, when comparing these results with those based on computation, good qualitative agreement was found.

Because MinD proteins are membrane-associated proteins (Raychaudhuri 2000), they are most likely to appear very near the cytoplasmic membrane by a polymerization mechanism mediated by the carboxy-terminus group (Taghbalout et al. 2006). In this regard,

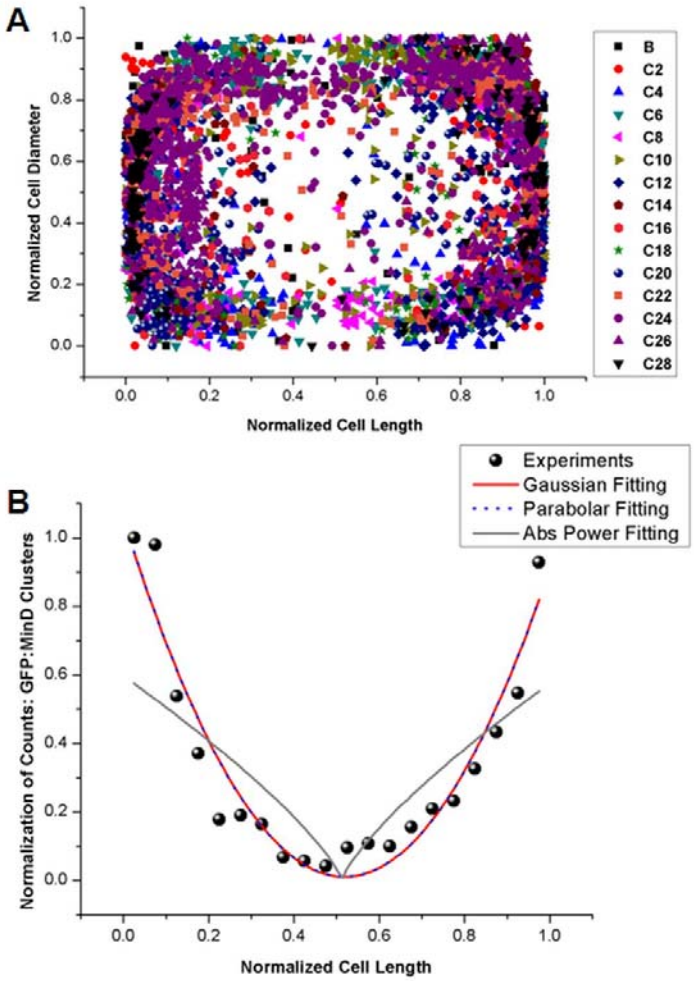

Fig. 6. The scattering behavior and distribution of GFP:MinD cluster positions. (**A**) Scattered plot of GFP:MinD cluster position for 15 cell samples in term of normalized cell length and cell diameter. (**B**) Fitting the spatial distribution of MinD proteins with the normalized cell length with 3 functions such as Gaussian function, parabola function and absolute power function. We found that Gaussian and parabola function can be fitted the experimental data with R-Square approximately 0.91.

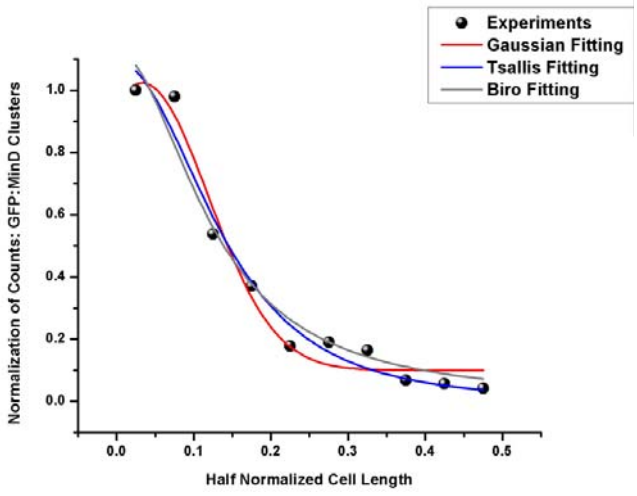

Fig. 7. The spatial distribution of GFP:MinD cluster proteins along the half normalized cell length. We fitted this distribution with 3 functions which are Gaussian function, Tsallis function, and Biro function. The fitting parameters are shown in Table 3. The difference of these functions is separated by the degree of correlation. Gaussian function performs the short correlation while Tsallis and Biro function are indicated the long range correlation via the 'q-values'. The spatial distribution best fitted with both Gaussian and Tsallis function with R-square approximately 0.97.

the major characteristic of MinD dynamics are distinguished not only by the trademark oscillatory pattern between the polar zones, but also by the membrane polar occupation pattern or horseshoe structure in the polar zone (Rowland et al. 2000; Rothfield 2005), as shown in Figure 6A for 13 cell samples. From this figure we analyzed the scattered position data on the normalized cell length and fit curve with 3 functions such as parabola, Gaussian, and absolute power function (Fig. 6B). The best fit functions are the parabola and the Gaussian function with R-square approximately 0.91. We found that these fitting function cloud be indicated the possible division size approximately 52% of the cell length (or near the midcell). This result corresponds to the placement of FtsZ ring at or near the midcell approximately 50% of cell position (Yu & Margolin 1999). In addition, we have fitted the half-length spatial distribution to both the normal distribution and the Tsallis distribution (Fig. 7). The differences between these distributions are at the root of statistical conception. Tsallis distribution focuses on the parameter q-values which describe the degree of correlation, while normal distribution is based on shot correlation. Moreover, normal distribution implies that MinD pro-

Table 2. The physical properties of the ensemble GFP:MinD dynamics.

Properties	Mean values	S.D.
Oscillation period (s)	54.8	8.6
Switching velocity (μm/s)	2.95	0.31
Localization velocity (μm/s)	0.29	0.06
Localization time (s)	27.4	4.97

Table 3. Functions and fitting parameters illustrated in Figure 7.

Gaussian	$y = y_0 + \frac{A}{w\sqrt{\frac{\pi}{2}}} e^{-2\frac{(x-x_c)^2}{w^2}}$	
Adj. R-Square	0.97	
	Parameters	Value
	y_0	0.10
	x_c	0.03
	w	0.17
	A	0.2
Tsallis	$y = A_q \left[1 - (1-q)\frac{\beta_m x^2}{2}\right]^{\frac{1}{1-q}}$	
Adj. R-Square	0.97	
	Parameters	Value
	A_q	1.01
	q	1.58
	β_m	47.14
Biro	$y = f_0 \left(1 + (q-1)Bx^2\right)^{\frac{q}{(1-q)}}$	
Adj. R-Square	0.95	
	Parameters	Value
	f_0	1.12
	q	−151676
	B	−4.26E-04

teins are transported through normal diffusion. In this regard, several models of Min protein dynamics have been based on the ordinary diffusion hypothesis. Recently Kulkarni et al. (2004) proposed a pattern formation of MinD molecules which is based on the normal distribution function. Because our data can nicely be fitted with the Tsallis distribution – which can describe the distribution of MinD proteins in terms of correlation degree or q-values – this may indicate a relationship to the MinD polymerization mechanism near the cytoplasmic membrane. We would like to mention that most or all experimental protocols could not quantitatively reveal the localization characteristics of MinD. Again, this graph quantitatively presents the distribution of MinD, although it was previously qualitatively reported (Hu & Lutkenhaus 1999; Raskin & de Boer 1999a,b; Hale et al. 2001) that MinD protein concentration is lowest at the midcell. Moreover, mathematical modeling and simulation results (Howard et al. 2001; Meinhardt & de Boer 2001; Kruse 2002; Howard & Rutenberg 2003; Huang et al. 2003; Drew et al. 2005; Meacci & Kruse 2005; Modchang et al. 2005) could also be validated and confirmed using our experimental results. It is surprising, however, that no report has shown a precise space-time plot and associated trajectories. It may be important to point out that Gaussian function fitting may imply that MinD dynamics is mediated by the concentration gradient-driven force of MinD (or more precisely, the MinCDE system). It is possible that this graph could be used to determine the precise locations of the midcell zone domain and the polar zone domain. If so, this must be done with care, and relevant biological considerations should be taken into account. The summary of the quantitative findings of localization and delocalization by using STT is given in Table 2. Lastly, it may be reasonable to say that our approach could provide accurate enough predictions and suggests useful biological features in protein localization prediction.

Velocity distribution and anomalous diffusion

Focusing on velocities and velocity distribution of the dynamics, among the most interesting dynamic characteristics of MinD clusters are the differences in behavior between polar zones (trapping events) and midcell zone (flight events). These results are strongly related to the mechanism of MinE protein, which stimulates MinD ATPase activity (Hu et al. 2001; Suefuji et al. 2002). In MinD protein studies, the switching period is very difficult to detect using intensity spot-tracking. This is mainly because the GFP:MinD rapidly binds and rebinds and spreads to another pole. This phenomenon could be supported by the biochemical rate interaction for MinDE to MinD:ADP and MinE, and the nucleotide exchange from MinD:ADP to MinD:ATP in the cytoplasm (Fange & Elf 2006). Figure 8 shows the velocity distribution of GFP:MinD clusters throughout the *E. coli* cells (13 cell samples). Figure 8A presents a histogram of the velocity distribution of GFP-MinD clusters using all data sets (all 13 cells), while combined overlay of all individual is shown in the inset. To understand the dynamics governing this velocity distribution, we select a typical individual cell and plot the velocity distribution (Fig. 8B). We then fitted the graph by Gaussian distribution function (green dash, dot, dot)

$$y = y_0 + \frac{A}{w\sqrt{\frac{\pi}{2}}} e^{-2\frac{(v-v_c)^2}{w^2}}$$

and Tsallis distribution (red dash, dot, dot)

$$F_q(v) = A_q \left[1 - (1-q)\frac{\beta_m v^2}{2}\right]^{\frac{1}{1-q}}.$$

From curve fitting data, it is seen that the Tsallis distribution function (Upadhyaya 2001; Thurner 2003) fitted to our data sets better than did the Gaussian function, as shown in Figure 8B in which the Gaussian functions was not able to cover some data points. This was confirmed by the R-squared values. For the Tsallis distribution function, R-squared values are approximately

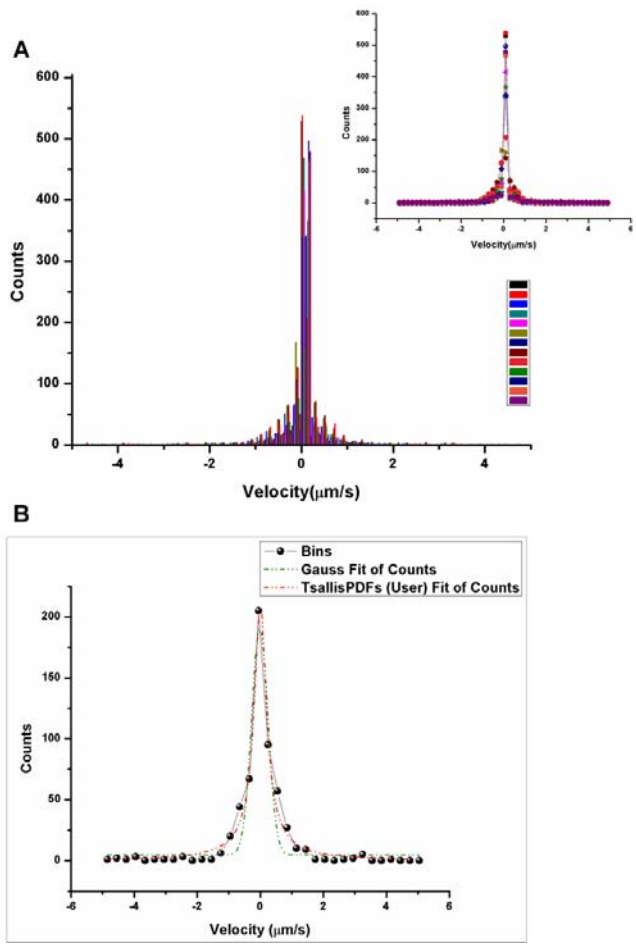

Fig. 8. The velocity distribution of GFP:MinD cluster throughout the *E. coli* cells (13 cell samples). (**A**) The histogram plot for GFP:MinD cluster that corresponds to the data sets in Figure 3B. The bin center of histogram (bin size = 0.2 μm/s) in each *E. coli* cell as shown in the small figure. (**B**) An example of velocity distribution analysis that compared between Gaussian distribution (green dash dot dot) and Tsallis distribution (red dash dot dot). The R-square values are approximately 0.95 for Gaussian curve fitting and 0.99 for Tsallis curve fitting. The highest distribution point is approximately -0.05 μm/s.

0.99 ± 0.01, while those of the Gaussian distribution function are approximately 0.97 ± 0.02. We reconfirmed that the mean of R-squared values from Tsallis function fitting is significantly higher than that from Gaussian function ($p = 0.0028$ by ANOVA test). According to the Tsallis distribution function, q-values indicate the correlation of particle motion. In our experiments, q-values are approximately 1.85 ± 0.28. The relation between q-values and dynamic exponents in anomalous diffusion is: $\alpha = 2/(1+q)$ (Fuentes et al. 2008). Our q-value is related to the dynamic exponent in anomalous subdiffusion where $\alpha = 0.7 \pm 0.08$, and related to the dynamic exponents from power spectrum density (PSD) throughout the *E. coli* cells where $\alpha = 0.64$. Based on our experiments, we suggest that the velocity distribution may imply non-Gaussian statistics. Since GFP-MinD clusters are in such close contact with the cytoplasmic membrane due to the polymerization mechanism, they cannot move independently. This biological evidence is believed to cause the anomalous subdiffusion which is indicated by the correlation of motion via q-values.

Based on the differences in time scale and dynamics between trapping and flight events, we then compartmentize a cell into two regions, namely mid-cell region and polar region. Since localization and self-organization are believed to play significant role in polar regions, we performed an analysis of the protein dynamics while MinD is localized at polar zones. We characterized the localized motion by measuring the mean squared displacement (MSD) of GFP-MinD clusters as a function of time lag, τ. Figure 9A,B are plotted in linear and log-log scale, respectively. In Figure 9B, the deviation bar represents the range of MSD deviation. This graph includes only 22 data points. Blue spots indicate the selected data points, and the red line indicates the linear curve. It reveals the power law, $\left\langle |\Delta\vec{r}|^2 \right\rangle \propto \tau^\alpha$ as expected (Saxton 1996; Tolic-Nørrelykke et al. 2004; Golding & Cox 2006), with $\alpha = 0.34 \pm 0.18$ and $R^2 = 0.98$ (13 individual cells). From diffusive motion theory, if $\alpha = 1$, this case indicates the normal diffusion or Brownian motion, while $0 < \alpha < 1$ perform subdiffusive motion (Metzler & Klafter 2000; Havlin et al. 2002; Wong et al. 2004). This suggests that the GFP:MinD cluster motion at the polar zones performs subdiffusion for the time scale approximately 27 seconds (see Table 2). This time scale corresponds to the half oscillation period of GFP:MinD. This implies that the trapping event is considerably dominated in MinD oscillation. By fitting the MSD with diffusive power law equation, we can find the distribution of the diffusion coefficient D to characterize the motion. From the distribution of D of subdiffusive motion (Fig. 9C), the distribution was fitted by Gaussian distribution. It is seen that D tends to favor the smaller values with respect to Gaussian function. This does make sense for the subdiffusion in comparison with normal diffusion. This is mainly because this subdiffusion arises when MinD interacts with the complex cellular medium or MinD experiences particle/obstacle reaction.

Figure 9D shows the log-log plot of PSD data points of GFP-MinD trajectories at the polar zones. The deviation bar represents the range of PSD deviation. The red line represents the linear fitting with a slope approximately -1.3 ± 0.16 and $R^2 = 0.82$. The power spectrum measures the characteristic of particle motion via the cluster GFP:MinD trajectories. The PSD is equal to the Fourier transformation of the autocorrelation function, and it characterizes the particle's "memory" of its previous position (Mantegna et al. 2000; Golding & Cox 2006). We assume the power spectrum obeys the power law corresponding to $P(f) \propto f^{-\nu}$ where $\nu = 1 + \alpha$ (Mantegna et al. 2000; Tolic-Nørrelykke et al. 2004; Golding & Cox 2006). If $\nu = 2$ ($\alpha = 1$), it indicates that the dynamics of the system is the normal diffusion or Brownian motion, whereas $0 < \alpha < 1$ the motion performs the subdiffusion (Metzler & Klafter 2000; Wong et al. 2004). Here we found

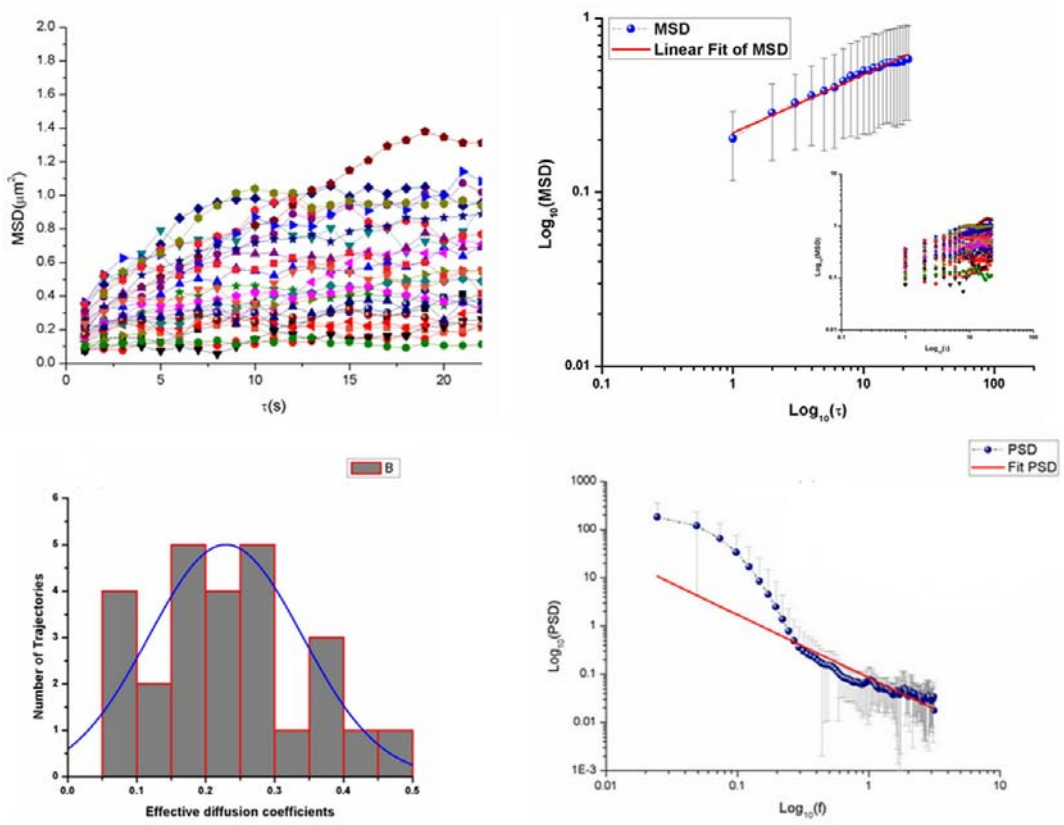

Fig. 9. Mean squared displacement (MSD), $\left\langle |\Delta\vec{r}|^2 \right\rangle$ of GFP:MinD cluster as a function of time lag and its PSD at the polar zones. (**A**) The MSD versus time for 26 trajectories (13 cell samples)**.** (**B**) The log-log plot of MSD at the polar zones, the deviate bar represents the ranging of MSD deviation. This graph is selected only 22 data points. Blue spots indicate the selected data points, red line indicates the linear curve fitting with a slope approximately 0.34 ± 0.18 and $R^2 = 0.98$. The small figure shows all MSD of individual trajectories at the same data points**.** (**C**) The log-log plot of PSD data points of GFP:MinD trajectories at the polar zones. The deviate bar represents the ranging of PSD deviation. The red line represents the linear fitting with a slope approximately −1.3 ± 0.16 and $R^2 = 0.82$. (**D**) The histogram of effective diffusion coefficients (EDC) compared with Normal Distribution in Blue line. The averages of EDCs are approximately 0.29 ± 0.11(μm^2/s$^\alpha$: $\alpha \sim 0.34 \pm 0.18$).

that the exponents of PSD in the cases of GFP:MinD cluster motion at polar zone are approximately 1.3 ± 0.16. Hence it indicated the long-range correlated random process (power-law correlation) with $0 < \nu < 2$ (Mantegna et al. 2000) which related to the subdiffusion. This exponent value is related to the subdiffusion dynamic exponent under the relation $\nu = 1 + \alpha$. Therefore, in our case, both exponents correspond to $\alpha \sim 0.3$. We suggest that the GFP-MinD cluster trajectory not only belongs to the subdiffusion type but also indicates the time memory of its motion. Recently there was experimental evidence by Golding & Cox (2006) that supported the subdiffusive motion of the mRNA molecules in *E. coli* cell with the dynamic exponent $\alpha = 0.7 \pm 0.07$. They suggested that the sources of cytoplasmic subdiffusion are independent of the main cytoskeletal elements (MreB and FtsZ). It could be explained by extremely crowded environment of the cytoplasm.

For the dynamics of GFP:MinD cluster, the subdiffusive motion may be described via the membrane association of MinD which is mediated by a carboxy-terminal membrane-targeting sequence (MTS) that varies between 8 and 12 amino acids in different species (Szeto et al. 2002; Hu et al. 2003). The MTS is attracted by electrostatics of its positively charged amino acids with the anionic lipid-enriched domain especially at the polar zones. These suggest that it can target the MinD protein moving to lipid bilayers (Hu et al. 2002; Szeto et al. 2002). These behaviors lead to the possible mechanism which restricted the motion of clusters protein (seem to obstruction by immobile protein).

Non-parametric statistical analysis and noise considerations

It seems reasonable to be concerned about using spot tracking to measure MinD position, because it could be extremely sensitive to small fluctuations in the nearly uniform background. One might note that STT represents the location of the highest fluctuation, which may jump around within the cell. These fluctuations may be caused by photon shot noise or camera noise, without representing underlying biological dynamics; or they may be small fluctuations that are accurately detected in the biological sample. These could be issues of noise characteristics, image quality and enhancement (to be discussed below). Specifically, we have checked the difference between noise background and protein dynamics by marking spots whose positions are outside (1–4) and inside (5–7) the cell (Fig. 10A). The outside spots

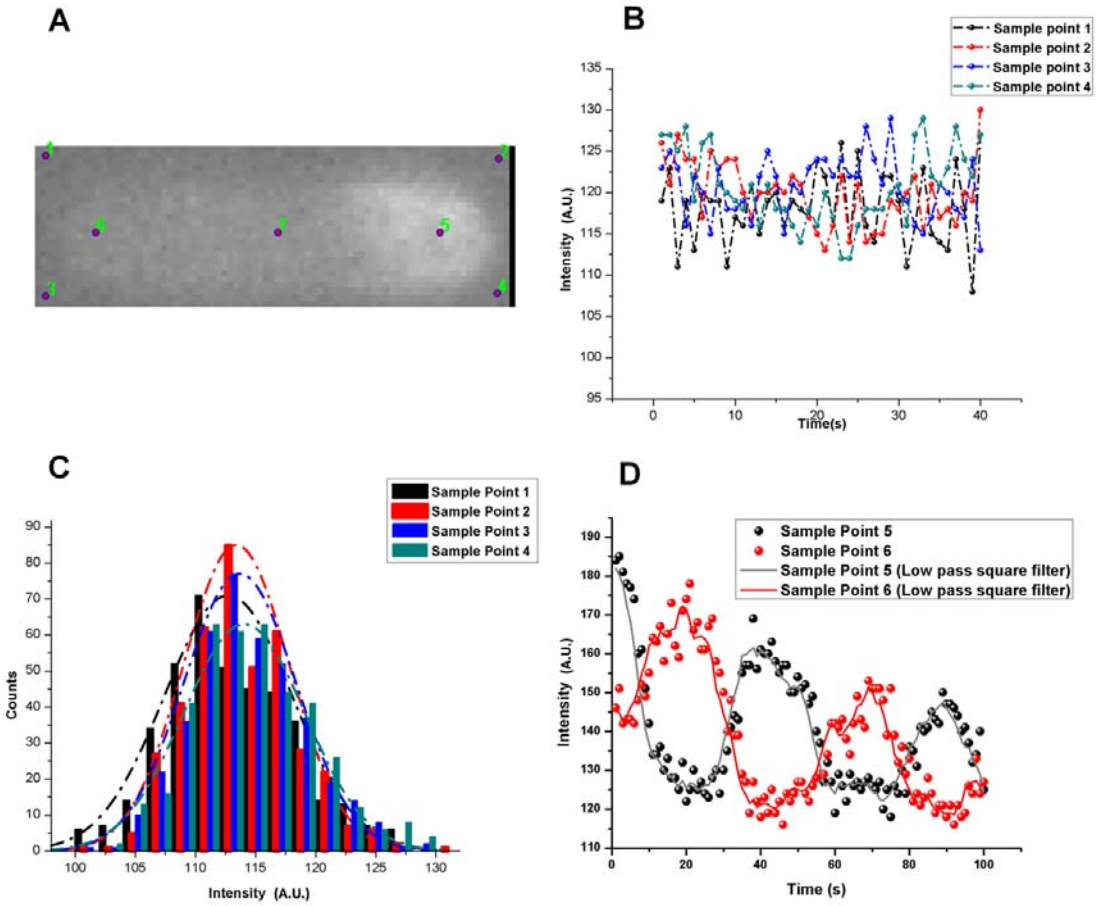

Fig. 10. The difference between noise backgrounds and GFP:MinD protein dynamics. (**A**) The marker points are detected the temporal intensity signals outside (1–4) and inside (5–7) an *E.coli* cell. (**B**) The temporal intensity signals outside the cell perform the noise background of image sequence. (**C**) The histogram for the temporal intensity signal in (**B**). This figure shows the curve fitting in term of normal distribution for each intensity signals. (**D**) The temporal intensity signals inside the cell that performs the GFP:MinD protein dynamics. In order to characterize the protein dynamics, we used the low pass square filter to reduce noise. The characteristic of GFP:MinD dynamics at the polar zones are shown in gray and red line, respectively.

1–4 represent the background detections in time evolution; while the inside spots 5–7 include these dynamics together with possible noises inside the cell. Figure 10B,C (time-series and corresponding histograms, respectively) indicates that the noise backgrounds found outside the cell samples belong to a Gaussian-type distribution which most likely is due to thermal fluctuation associated with the systems and environments. To see how these noises may affect the signals or dynamics, we have used cells in the same batch as samples 1–4, and performed noise reduction with a low-pass square filter (5x1) (Sprague et al. 2004). It was uncovered that the GFP-MinD protein dynamics clearly perform the oscillation pattern (Fig. 10D). Because the raw image sequences were very noisy and because this could obviously perturb the protein dynamics (as shown in Figure 1), we thus adopted to clear the noisy image by using Gaussian filter, and to enhance the image again before using intensity spot-tracking. The demonstration of how image preparation and processing provide a reasonable dynamic outcome has been previously mentioned. The underlined findings are found that the noise seems to be sporadic and random, with no relation to Min protein oscillation fluorescence.

Given the apparently good quality of the data, one might ask if there is a better analytical method to represent the data. There are a variety of approaches one could try. For example, ensembles are often represented using statistical measures. If MinD protein distributions are not Gaussian, using parametric statistics may be questionable. Hence we used the data directly from fluorescent microscopy signal and analyzed via non-parametric statistical analysis. Here we concerned the simplest analysis, namely estimating the medium, mode, and center of mass of signal positions. Our goal was to find alternative ways of tracking the position of the protein signal, and compared them with the results analyzed previously using spot tracking. To do so, we firstly analyzed MinD protein distribution along the long axis, or cell length, in pixel scale using fluorescent intensity data analysis as used by Kulkarni et al. (2004), and found that the intensity distribution along the long axis is normal distribution (400 sample images) with 95% confidence (data not shown). We calculated the median, mode and mean (center of mass or centroid) of the signal intensity (data not shown). For the median, we applied the software from MATLAB to find the 50^{th} percentile or 2^{nd} quartile of these sorted data

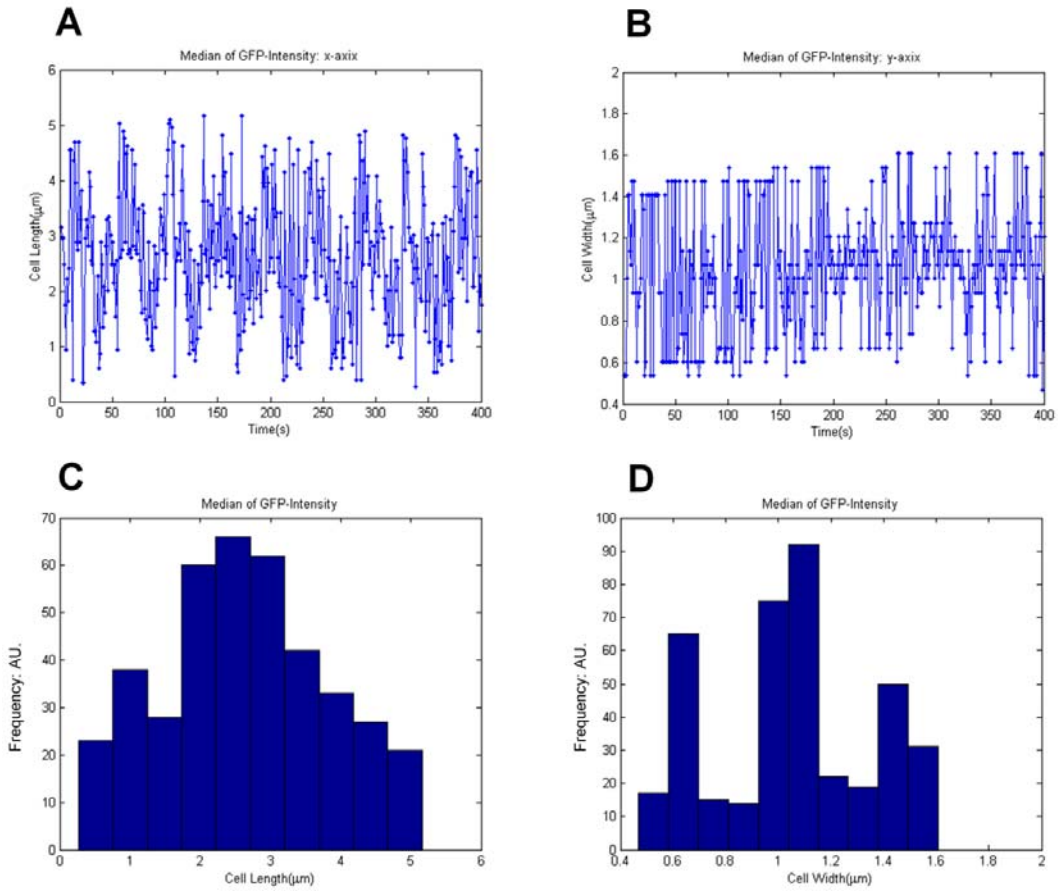

Fig. 11. The trajectory and histogram of GFP:MinD intensity position on x and y axis for Median case study. (**A**) and (**B**) The trajectory along x and y axis respectively. (**C**) and (**D**) The histogram for trajectory data that follow to the data sets in (**A**) and (**B**).

on the x (cell length) and y (cell width). The average of the medium (13 cells) has a bell-shape with the maximum at around the midcell area (Fig. 11A–D). When compared with previous experimental findings, it appeared that this statistics, mean is not consistent with the well-known theory, pole-to-pole dynamics of MinD. In contrast, the mode (Fig. 12A–D) appears to capture the pole-to-pole and localization dynamics which is very much consistent with those experiments and theories (see also Figure 5). In addition, we also calculated the mean intensity dynamics in terms of center of mass or centroid (Fish et al. 2004), as shown in Figure 13A–D. Though the mean seems to feature pole-to-pole switching dynamics as does the mode, the amplitude is relatively small. This obviously is due to the distributed mass or spreading nature of proteins in the cell. This in fact could lead to a misinterpretation of the details of MinD characteristics – especially the localization pattern. In summary, these analyses suggest that the statistic parameter, the mode obtained from the direct fluorescence microscopy data, is in a good agreement with that obtained by STT. Indeed it should be surprising because both two statistical values are very similar in computational methodology.

Concluding remarks

The goal of this report was to propose the application of STT to study MinD dynamics; in other words, to use computer-aided image analysis of fluorescence microscopy data. STT was used for tracking the maximum of the distribution of a particle ensemble, but not for a single molecule. In other words, they are likely tracking a constantly reorganizing accumulation of MinD proteins. The main results are twofold: (i) the demonstration of how STT could be an acceptable tool for MinD dynamics studies; and (ii) quantitative findings with parametric and non-parametric analyses. From our experimental results, the ascertainment of ensemble MinD position can be used to characterize and analyze specific positions, paths or trajectories, spatial distribution, pole-to-pole switching, localization, periods, and global dynamic pattern formation. To our knowledge, this is the first report delivering the MinD dynamics observation both qualitatively and quantitatively. With STT, all results were qualitatively found to agree with previous experimental and theoretical results. Moreover, more precise quantitative information regarding MinD dynamics has also been obtained. For example, our measured oscillation period is 54.6 ± 8.6 s, which is a standard value of the MinD period of oscillation for bacteria of this size and strain. Moreover, due to the nature of noise interference, it is believed that a Gaussian blur filter should be sufficient to reduce the noise effect. However, noise suppression and filter optimization should be pursued in the near future. As a result, we have performed a non-parametric analysis to

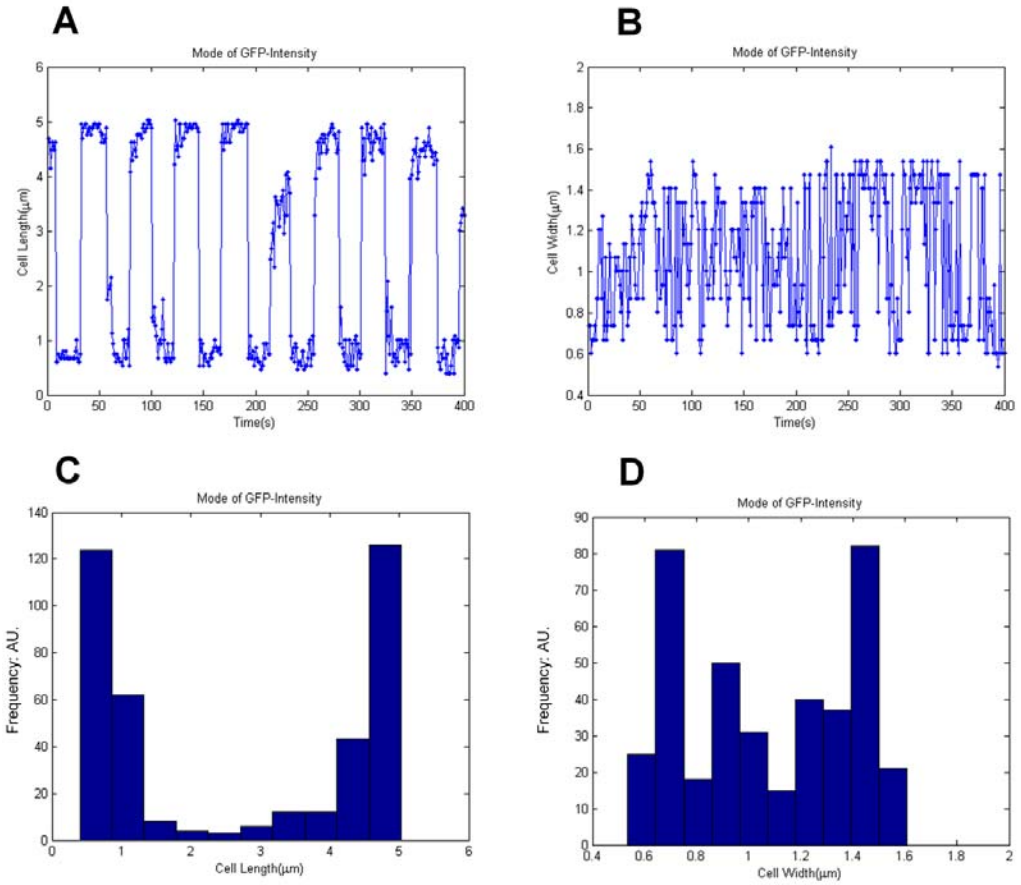

Fig. 12. The trajectory and histogram of GFP:MinD intensity position on x and y axis for Mode case study. (**A**) and (**B**) The trajectory along x and y axis, respectively. (**C**) and (**D**) The histogram for trajectory data that follow to the data sets in (**A**) and (**B**).

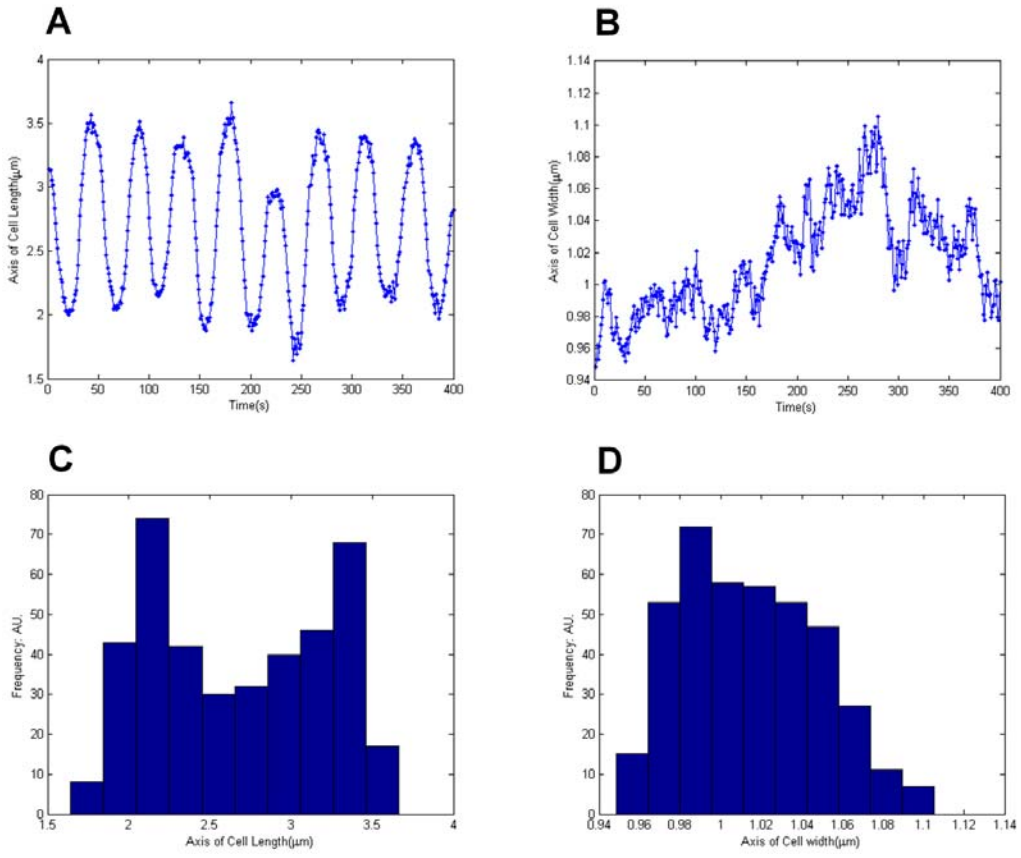

Fig. 13. The trajectory and histogram of GFP:MinD intensity position on x and y axis for Mean or centriod case study. (**A**) and (**B**) The trajectory along x and y axis, respectively. (**C**) and (**D**) The histogram for trajectory data that follow to the data sets in (**A**) and (**B**).

compare with the parametric one, in order to reveal our findings in various aspects.

It is reasonable to conclude that the measurements performed are more accurate than, e.g., eye-observed measurement in two-dimensional image sequences. However, the accuracy of STT may be subject to several environmental factors. With further improvements to STT, especially applications in three dimensions, the information gained may reflect such mechanisms as the obstruction of MinD by other mobile or immobile molecules, or by other Min proteins; the binding and obstruction by cellular components; and so on. For future application, we plan to use the same techniques to investigate other Min protein types, such as MinE or others. In addition, some important properties of Min proteins – such as transport properties, energy landscape, effect of external stresses, etc. – warrant further investigation. Lastly, we believe that the STT will be widely applied to Min protein systems in the very near future. Moreover, with improvements in STTs, like data acquisition and data analysis, STT could become very well-accepted technique. The three-dimensional, true-to-life results are unambiguously what we strive for. Furthermore, the combined use of STT and the well-known technique of fluorescent labeling or dyeing could be a promising alternative to other types of labeling, including the nanoparticle labeling approach.

Acknowledgements

Firstly, we would like to thank the anonymous referee who provided such very useful comments regarding our work. This contributed greatly to the quality of our paper. We would like to thank Prof. Lawrence Rothfield and Dr. Yu-Ling Shih (Department of Microbiology, University of Connecticut Health Center) for kindly providing *E. coli* RC1/pFX9 [$\Delta min/P_{lac}$-*gfp*::$\Delta minD$ $\Delta minE$] for our use. Special thanks also go to the Commission on Higher Education for the CHE-PhD-THA Program Scholarship to Paisan Kanthang and to the Development and Promotion of Science and Technology Talent Project Scholarship to Waipot Ngamsaad. This work was supported by the National Center for Genetic Engineering and Biotechnology (BIOTEC), The Thailand Research Fund (TRF), the Commission on Higher Education (CHE), the Thailand Center of Excellence for Physics (ThEP), and the Software Industry Promotion Agency (SIPA) of Thailand.

References

Babcock H.P., Chen C. & Zhuang X. 2004. Using single-particle tracking to study nuclear trafficking of viral genes. Biophys. J. **87:** 2749–2758.

de Boer P.A.J., Crossley R.E., Hand A.R. & Rothfield L.I. 1991. The MinD protein is a membrane ATPase required for the correct placement of the *Escherichia coli* division site. EMBO J. **10:** 4371–4380.

de Boer P.A.J., Crossley R.E. & Rothfield L.I. 1989. A division inhibitor and a topological specificity factor coded for by the minicell locus determine proper placement of the division septum in *E. coli*. Cell **56:** 641–649.

Drew D.A., Osborn M.J. & Rothfield L.I. 2005. A polymerization-depolymerization model that accurately generates the self-sustained oscillatory system involved in bacterial division site placement. Proc. Natl. Acad. Sci. USA **102:** 6114–6118.

Fange D. & Elf J. 2006. Noise-induced Min phenotypes in *E. coli*. PLoS Comput. Biol. **2:** e80.

Fish A., Akselrod D. & Yadid-Pech O. 2004. High precision image centroid computation via an adaptive k-winner-take-all circuit in conjunction with a dynamic element matching algorithm for star tracking applications. Analog Integrated Circuits and Signal Processing **39:** 251–266.

Fuentes M.A. & Cáceres M.O. 2008. Computing the non-linear anomalous diffusion equation from first principles. Physics Lett. A **372:** 1236–1239.

Golding I. & Cox E. C. Physical nature of bacterial cytoplasm. 2006. Phys. Rev. Lett. **96:** 098102.

Hale C.A., Meinhardt H. & de Boer P.A. 2001. Dynamics localization cycle of the cell division regulator MinE in *Escherichia coli*. EMBO J. **20:** 1563–1572.

Havlin S. & ben-Avraham D. 2002. Diffusion in disordered media. Advan. Phys. **51**: 187–292.

Howard M., Rutenberg A.D. & de Vet S. 2001. Dynamics compartmentalization of bacteria: accurate division in *E. coli*. Phys. Rev. Lett. **87:** 278102.

Howard M. & Rutenberg A.D. 2003. Pattern formation inside bacteria: fluctuations due to the low copy number of proteins. Phys. Rev. Lett. **90:** 128102.

Hu Z., Gogol E.P. & Lutkenhaus J. 2002. Dynamics assembly of MinD on phospholipid vesicles regulated by ATP and MinE. Proc. Natl Acad. Sci. USA **99:** 6761–6766.

Hu Z. & Lutkenhaus J. 1999. Topological regulation of cell division in *Escherichia coli* involves rapid pole to pole oscillation of the division inhibitor MinC under the control of MinD and MinE. Mol. Microbiol. **34:** 82–90.

Hu Z. & Lutkenhaus J. 2001. Topological regulation of cell division in *E. coli*: spatiotemporal oscillation of MinD requires stimulation of its ATPase by MinE and phospholipid. Mol. Cell **7:** 1337–1343.

Hu Z. & Lutkenhaus J. 2003. A conserved sequence at the C-terminus of MinD is required for binding to the membrane and targeting MinC to the septum. Mol. Microbiol. **47:** 345–355.

Huang K.C., Meir Y. & Wingreen N.S. 2003. Dynamic structures in *Escherichia coli*: spontaneous formation of MinE rings and MinD polar zones. Proc. Natl. Acad. Sci. USA **100:** 12724–12728.

Justice S.S., Garcia-Lara J. & Rothfield L.I. 2000. Cell division inhibitors SulA and MinC/MinD block septum formation at different steps in the assembly of the *Escherichia coli* division machinery. Mol. Microbiol. **37:** 410–423.

Kerr R.A., Levine H., Sejnowski T.J. & Rappel W.J. 2006. Division accuracy in a stochastic model of Min oscillations in Escherichia coli. Proc. Natl. Acad. Sci. USA **103:** 347–352.

Kim S.Y., Gitai Z., Kinkhabwala A., Shapiro L. & Moerner W.E. 2006. Single molecules of the bacterial actin MreB undergo directed treadmilling motion in *Caulobacter crescentus*. Proc. Natl. Acad. Sci. USA **103:** 10929–10934.

Kruse K. 2002. A dynamic model for determining the middle of *Escherichia coli*. Biophys. J. **82:** 618–627.

Kulkarni R.V., Huang K.C., Kloster M. & Wingreen N.S. 2004. Pattern formation within *Escherichia coli*: diffusion, membrane attachment, and self-interaction of MinD molecules. Phys. Rev. Lett. **93:** 228103.

Lutkenhaus J. 2007. Assembly dynamics of the bacterial MinCDE system and spatial regulation of the Z ring. Annu. Rev. Biochem. **76:** 539–562.

Lutkenhaus J. & Addinall S.G. 1997. Bacterial cell division and the Z ring. Annu. Rev. Biochem. **66:** 93–116.

Mantegna R.N. & Stanley H.E. 2000. An Introduction to Econophysics Correlations and Complexity in Finance. Cambridge University Press, Cambridge, England, 144 pp.

Meacci G. & Kruse K. 2005. Min-oscillations in Escherichia coli induced by interactions of membrane-bound proteins. Phys. Biol. **2:** 89–97.

Meinhardt H. & de Boer P.A. 2001. Pattern formation in *Escherichia coli*: a model for the pole-to-pole oscillations of Min proteins and the localization of the division site. Proc. Natl. Acad. Sci. USA **98:** 14202–14207.

Metzler R. & Klafter J. 2000. The random walk's guide to anomalous diffusion: a fractional dynamics approach. Phys. Rep. **339:** 1–77

Modchang C., Kanthang P., Triampo W., Ngamsaad W., Nuttawut N. & Tang I.M. 2005. Modeling of the dynamics pole-to-pole oscillations of the Min proteins in bacterial cell division: the effect of an external field. J. Korean Phys. Soc. **46:** 1031–1036.

Pavin N., Paljetak H.C. & Krstić V. 2006. Min-protein oscillations in *Escherichia coli* with spontaneous formation of two-stranded filaments in a three-dimensional stochastic reaction-diffusion model. Phys. Rev. E **73:** 021904.

Qian H., Scheetz M. & Elson E.L. 1991. Single particle tracking. Biophys. J. **60:** 910–921.

Raskin D.M. & de Boer P.A. 1999a. MinDE-dependent pole-to-pole oscillation of division inhibitor MinC in *Escherichia coli*. J. Bacteriol. **181:** 6419–6424.

Raskin D.M. & de Boer P.A. 1999b. Rapid pole-to-pole oscillation of a protein required for directing division to the middle of *Escherichia coli*. Proc. Natl. Acad. Sci. USA **96**: 4971–4976.

RayChaudhuri D., Gordon G.S. & Wright A. 2000. How does a bacterium find its middle? Nat. Struct. Biol. **7:** 997–999.

Rothfield L., Justice S. & Garcia-Lara J. 1999. Bacterial cell division. Annu. Rev. Genet. **33:** 423–448.

Rothfield L.I., Shih Y.L. & King G. 2001. Polar explorers: membrane proteins that determine division site placement. Cell **106:** 13–16.

Rothfield L., Taghbalout A. & Shih Y.L. 2005. Spatial control of bacterial division-site placement. Nat. Rev. Microbiol. **31:** 959–968.

Rowland S.L., Fu X., Sayed M.A., Zhang Y., Cook W.R. & Rothfield L. 2000. Membrane redistribution of the *Escherichia coli* MinD protein induced by MinE. J. Bacteriol **182:** 613–619.

Sage D., Neumann F.R., Hediger F., Gasser S.M. & Unser M. 2005. Automatic tracking of individual fluorescence particles: application to the study of chromosome dynamics. IEEE Trans. Image Process. **14:** 1372–1383.

Saxton M.J. 1996. Anomalous diffusion due to binding: a Monte Carlo study. Biophys. J. **70:** 1250–1262.

Saxton M.J. & Jacobson K. 1997. Single-particle tracking: applications to membrane dynamics. Annu Rev. Biophys. Biomol. Struct. **26:** 373–399.

Shih Y.L., Le T. & Rothfield L. 2003. Division site selection in *Escherichia coli* involves dynamic redistribution of Min proteins within coiled structures that extend between the two cell poles. Proc. Natl Acad. Sci. USA **100:** 7865–7870.

Suefuji K., Valluzzi R. & RayChaudhuri D. 2002. Dynamic assembly of MinD into filament bundles modulated by ATP, phospholipids, and MinE. Proc. Natl Acad. Sci. USA **99:** 16776–16781.

Szeto J., Eng N.F., Acharya S., Rigden M.D. & Dillon J.A. 2005. A conserved polar region in the cell division site determinant MinD is required for responding to MinE-induced oscillation but not for localization within coiled arrays. Res. Microbiol. **156:** 17–29.

Szeto T.H., Rowland S.L., Rothfield L.I. & King G.F. 2002. Membrane localization of MinD is mediated by a C-terminal motif that is conserved across eubacteria, archaea, and chloroplasts. Proc. Natl Acad. Sci. USA **99:** 15693–15698.

Taghbalout A., Ma L. & Rothfield L. 2006. Role of MinD-membrane association in Min protein interactions. J. Bacteriol. **188:** 2993–3001.

Thurner S., Wick N., Hanele R., Sedivy R. & Huber L. 2003. Anomalous diffusion on dynamical networks: a model for interacting epithelial cell migration. Physica A **320:** 475–484.

Tolic-Nørrelykke I.M., Munteanu E.L. & Thon G. 2004. Anomalous diffusion in living yeast cells. Phys. Rev. Lett. **93:** 078102.

Tostevin F. & Howard M. 2006. A stochastic model of Min oscillations in *Escherichia coli* and Min protein segregation during cell division. Phys. Biol. **3:** 1–12.

Touhami A., Jericho M. & Rutenberg A.D. 2006. Temperature dependence of MinD oscillation in *Escherichia coli*: running hot and fast. J. Bacteriol. **188:** 7661–7667.

Upadhyaya A., Rieub J.P., Glaziera J.A. & Sawada Y. 2001. Anomalous diffusion and non-Gaussian velocity distribution of Hydra cells in cellular aggregates. Physica A **293:** 549–558.

Woldringh C.L., Mulder E., Huls P.G. & Vischer N. 1991. Toporegulation of bacterial division according to the nucleoid occlusion model. Res. Microbiol**. 142:** 309–320.

Wong I.Y., Gardel M.L., Reichman D.R., Weeks E.R., Valentine M.T., Bausch A. R. & Weitz D.A. 2004. Anomalous diffusion probes microstructure dynamics of entangled F-actin networks. Phys. Rev. Lett. **92:** 178101.

Yu X.C. & Margolin W. 1999. FtsZ ring clusters in Min and partition mutants: role of both the Min system and the nucleoid in regulating FtsZ ring localization. Mol. Microbiol**. 32:** 315–326.

Received January 16, 2008
Accepted October 24, 2008